Inorg. Chem. **2003**, *42*, 8449–8455

Inorganic Chemistry
Article

Theoretical Studies of the Complex $[(BPMEN)Fe(II)(NCCH_3)_2]^{2+}$, Precursor of Non-Heme Iron Catalysts for Olefin Epoxidation and Cis-Dihydroxylation

David Quiñonero, Djamaladdin G. Musaev,* and Keiji Morokuma*

Cherry L. Emerson Center for Scientific Computation and Department of Chemistry,
Emory University, Atlanta, Georgia 30322

Received July 17, 2003

The density functional theory (DFT) was applied to elucidate the electronic structure of the BPMEN [*N*,*N*′-bis(6-*R*-2-pyridylmethyl)-1,2-diaminoethane] iron complex, $[(BPMEN)Fe(NCCH_3)_2]^{2+}$, a precursor of catalysts that catalyze the stereospecific olefin oxidation. The low-lying high and low spin states of complex **1** (R = H) are nearly degenerate with a slight preference for the high spin state. For complexes with substituents (R) at the 6-positions of two pyridine rings of BPMEN, the ground state is the high spin (HS) state, with the low spin (LS) state higher in energy by 9.5, 5.3, 8.5, 6.3, and 5.1 kcal/mol for complexes **2** ($R = CH_3$), **3** ($R = SiH_3$), **4** (R = OH), **5** (R = F), and **6** (R = CN), respectively, with the B3LYP method. Our findings for complexes **1** and **2** are in good agreement with the experimental observations. The calculated LS–HS difference of 17.9 kcal/mol for complex **7** (R = *t*-Bu) clearly demonstrates that the steric effect causes the Fe–N bonds to stretch and favors the high spin state. Comparison of the B3LYP and B3PW91 results with experiments and ab initio MP2 and CCSD(T) as well as pure DFT results shows that hybrid DFT methods provide a qualitatively correct description of the relative energies of low-lying electronic states of a model of the $[(BPMEN)Fe(NCCH_3)_2]^{2+}$ complex, while pure DFT methods underestimate the stability of the HS state.

1. Introduction

The non-heme iron-containing Rieske dioxygenases are the only ones among both heme and non-heme iron enzymes that are capable of carrying out enantioselective cis-dihydroxylation of arene and olefin double bonds.[1] The active site of one of these Rieske dioxygenases, the naphthalene 1,2-dioxygenase, consists of a mononuclear iron center coordinated by two histidines and a bidentate carboxylate group, with the remaining two cis sites available for exogenous ligand binding. To model the structure and reactivity of this enzyme, several non-heme iron catalysts for olefin oxidation have been synthesized,[2] among which the catalysts reported by Que and co-workers[2c−f] are still the only examples capable of olefin cis-dihydroxylation. Precursors of these catalysts are presented in Figure 1, which are the iron complexes of the tetradentate N4 ligands such as TPA [tris(2-pyridylmethyl)amine] and BPMEN [*N*,*N*′-bis-(2-pyridylmethyl)-1,2-diaminoethane]. One should note that the actual catalyst derived from complex **1** (Figure 1), after oxidizing it by hydrogen peroxide, is believed to be the Fe(III)(OOH)-type of compounds.[2e−f] Depending on the substituent (R) at the 6-position of the pyridine ring, these complexes show different physical properties, which could be related to the differences in their spin states. Indeed, experimental studies of the $[(BPMEN)FeX_2]^{2+}$ complexes (Figure 1), with either acetonitrile or triflate anion as X, show that complex **1** with R = H has a low spin Fe(II) center, while complex **2** with $R = CH_3$ has a high spin Fe(II) center.[2e] Furthermore, **1** exhibits a compact ^1H NMR spectrum[2e] at −40 °C. However, upon increasing the

---

* Corresponding authors. E-mail: dmusaev@emory.edu (D.G.M.); morokuma@emory.edu (K.M.).

(1) (a) Gibson, D. T.; Subramanian, V. *Microbial Degradation of Organic Compounds*; Gibson, D. T., Ed.; Marcel Dekker: New York, 1984; pp 181−251. (b) Wende, P.; Bernhardt, F.-H.; Pfleger, K. *Eur. J. Biochem.* **1989**, *181*, 189. (c) Lee, K.; Gibson, D. T. *J. Bacteriol.* **1996**, *178*, 3353. (d) Beil, S.; Happe, B.; Timmis, K. N.; Pieper, D. H. *Eur. J. Biochem.* **1997**, *247*, 190. (e) Lange, C. C.; Wackett, L. P. *J. Bacteriol.* **1997**, *179*, 3858. (f) Wolfe, M. D.; Parales, J. V.; Gibson, D. T.; Lipscomb, J. D. *J. Biol. Chem.* **2001**, *276*, 1945.

(2) (a) Nam, W.; Ho, R. Y. N.; Valentine, J. S. *J. Am. Chem. Soc.* **1991**, *113*, 7052. (b) Guajardo, R. J.; Hudson, S. E.; Brown, S. J.; Mascharak, P. K. *J. Am. Chem. Soc.* **1993**, *115*, 7971. (c) Chen, K.; Que, L. *Angew. Chem., Int. Ed.* **1999**, *38*, 2227. (d) Costas, M.; Tipton, A. K.; Chen, K.; Jo, D.-H.; Que, L. *J. Am. Chem. Soc.* **2001**, *123*, 6722. (e) Chen, K.; Costas, M.; Kim, J.; Tipton, A.; Que, L. *J. Am. Chem. Soc.* **2002**, *124*, 3026. (f) Chen, K.; Costas, M.; Que, L. *J. Chem. Soc., Dalton Trans.* **2002**, 672.

10.1021/ic0348392 CCC: $25.00 © 2003 American Chemical Society
Published on Web 10/30/2003

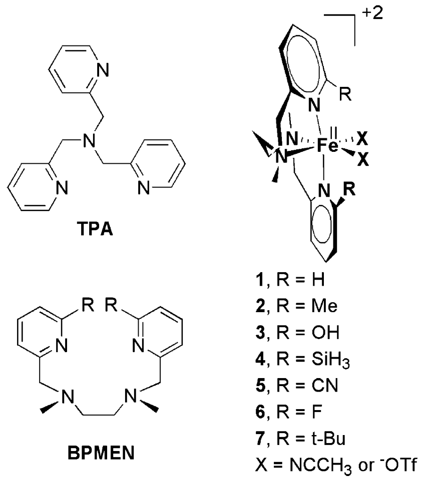

Figure 1. Tetradentate N4 TPA and BPMEN ligands. On the right-hand side, schematic representation of the studied complexes, consisting of an Fe(II) center coordinated by two acetonitrile molecules and BMPEN ligand with different R substitution.

temperature, the spectral window becomes monotonically larger, so that at 30 °C a spectrum spanning 90 ppm in chemical shift is observed. These results indicate that the Fe(II) center in **1** undergoes a transition from low spin to high spin in this temperature range. On the contrary, complex **2** exhibits a spectrum typical for high spin Fe(II) complexes with chemical shifts ranging from 120 to -50 ppm.

Thus, these experiments indicate that at low temperatures complex **1** with $R = H$ is a low spin Fe(II) complex, while at higher temperature it becomes a high spin complex. Meanwhile, complex **2** with $R = CH_3$ is a high spin Fe(II) complex at all the studied temperature range. This experimental result, as well as the observed difference in the reactivity of complexes **1** and **2**, makes it extremely important to elucidate the role of the substitution (R) in the pyridine ring of BPMEN in the electronic and geometric structures, as well as the reactivity of the $[(BPMEN)FeX_2]^{2+}$ catalyst. Answers for these questions could significantly facilitate understanding of the reported unique reactivity of the BPMEN−Fe based catalyst and, consequently, could help in designing new and more efficient catalysts for enantioselective cis-dihydroxylation of olefin. In this paper we elucidate the role of the substitution (R) on the pyridine ring of BPMEN in the electronic and geometric structures of the $[(BPMEN)FeX_2]^{2+}$ catalyst by using computational methods. Another important issue, the relation between low-lying spin states and the reactivity of BPMEN iron catalysts, will be addressed in a forthcoming paper.

2. Computational Methods

The present paper consists of three parts. The first part is the study of the geometry and energetics of different spin states of the catalysts **1** and **2**. We optimized the geometry of these catalysts using the restricted and unrestricted Kohn−Sham DFT.[3] In general, the Kohn−Sham Hamiltonian takes into account exchange and correlation effects.[4] However, to make spin polarization possible, one must apply a spin-unrestricted (U) formalism,[5,6] allowing α and β electrons to occupy orbitals with different energies and spatial localizations. Furthermore, the unrestricted Kohn−Sham wave function obtained from the SCF calculation is an eigenfunction of the S_z operator with the eigenvalue of M_S but is not an eigenfunction of the total spin operator S^2. As a consequence, the unrestricted singlet states are, in general, spin contaminated and can have strong admixtures from higher spin states[7] [i.e., $\langle S^2 \rangle > M_S(M_S + 1)$]. However, the high spin states can be well represented at the Kohn−Sham DFT level.[8]

In these calculations we used the B3LYP functional, which utilizes the three-parameter exchange functional of Becke[4a,9] in conjunction with the Lee−Yang−Parr[4b] correlation functional. The exchange functional in B3LYP constitutes a hybrid approach that combines Hartree−Fock[6,10] with Slater[3,11] and gradient-corrected Becke exchange.[4a,9a,b] The correlation in B3LYP is introduced by a combination of the local and nonlocal functionals of Vosko−Wilk−Nusair[9c] and Lee−Yang−Parr,[4b] respectively.

However, it is well established[12] that hybrid density functional approaches (such as B3LYP) overestimate the stability of high spin states relative to low spin states. Therefore, we also used the nonhybrid (or pure) density functional approach such as BLYP, which combines the Becke88 (B) exchange functional[9a] with the Lee−Yang−Parr[4b] correlation functional (exactly the same way as B3LYP does). To make this comparison more systematic, we employed two more density functional methods, hybrid B3PW91 and nonhybrid BPW91, utilizing the same B3 and B exchange functionals with the Perdew and Wang gradient-corrected correlation functional,[13] respectively. Also, we tested the PW91PW91 functional, which combines the Perdew and Wang exchange functional with their gradient-corrected correlation functional.[13]

In these calculations, the Huzinaga−Dunning all-electron double-ζ basis for H, C, and N and the Los Alamos effective core potential with associated double-ζ basis for Fe (LANL2DZ basis set)[14] were used. For comparison purposes, we also employed the all-electron basis sets such as 6-311G(d) and 6-311+G(d), in conjunction with the Fe basis optimized by Wachters[15] and Hay[16] using the scaling factors of Raghachavari and Trucks.[17] Unless

---

(3) Kohn, W.; Sham, L. J. *Phys. Rev.* **1965**, *140*, A1133.

(4) (a) Becke, A. D. *J. Chem. Phys.* **1993**, *98*, 5648. (b) Lee, C.; Yang, W.; Parr, R. G. *Phys. Rev. B* **1988**, *37*, 785. (c) Perdew, J. P.; Wang, Y. *Phys. Rev. B* **1992**, *45*, 13244.

(5) Parr, R. G.; Yang, W. *Density Functional Theory of Atoms and Molecules*; Oxford University: New York, 1989.

(6) Hehre, W. J.; Radom, L.; Schleyer, P. v. R.; Pople, J. A. *Ab Initio Molecular Orbital Theory*; Wiley: New York, 1986.

(7) Noodleman, L.; Case, D. A.; Baerends, E. J. *Density Functional Methods in Chemistry*; Labanowski, J. K., Andzelm, J. W., Eds.; Springer-Verlag, New York, 1991.

(8) (a) Hay, P. J.; Thibeault, J. C.; Hoffmann, R. J. *J. Am. Chem. Soc.* **1975**, *97*, 4884 . (b) Kahn, O. *Molecular Magnetism*; VCH: New York, 1993. (c) Noodleman, L. *J. Chem. Phys.* **1981**, *74*, 5737.

(9) (a) Becke, A. D. *Phys. Rev. A* **1988**, *38*, 3098−3100. (b) Becke, A. D. *J. Chem. Phys.* **1993**, *98*, 1372. (c) Vosko, S. H.; Wilk, L.; Nusair, M. *Can. J. Phys.* **1980**, *58*, 1200.

(10) (a) Hartree, D. R. *Proc. Cambridge Philos. Soc.* **1927**, *24*, 89. (b) Fock, V. *Physik* **1930**, *61*, 126. (c) Hartree, D. R. *The Calculation of Atomic Structure*; Wiley: New York, 1957.

(11) (a) Hohenberg, P.; Kohn, W. *Phys. Rev.* **1964**, *136*, B864. (b) Slater, J. C. *Quantum Theory of Molecules and Solids. Vol. 4: The Self-Consistent Field for Molecules and Solids*; McGraw-Hill: New York, 1974.

(12) Paulsen, H.; Duelund, L.; Winkler, H.; Toftlund, H.; Trautwein, A. X. *Inorg. Chem.* **2001**, *40*, 2201.

(13) Perdew, J. P.; Burke K.; Wang, Y. *Phys. Rev. B* **1996**, *54*, 16533.

(14) (a) Dunning, T. H., Jr.; Hay, P. J. In *Modern Theoretical Chemistry*; Schaefer, H. F., III, Ed.; Plenum: New York, 1976. (b) Hay, P. J.; Wadt, W. R. *J. Chem. Phys.* **1985**, *82*, 270.

(15) Wachters, A. J. H. *J. Chem. Phys.* **1970**, *52*, 1033.

(16) Hay, P. J. *J. Chem. Phys.* **1977**, *66*, 4377.

(17) Raghachavari, K.; Trucks, G. W. *J. Chem. Phys.* **1989**, *91*, 1062.

stated otherwise, optimized structures were confirmed to be local minima by performing analytical harmonic vibrational frequency analyses. The energies given in this paper do not include the zero point energy corrections.

Note that for the singlet electronic states both the restricted and unrestricted formalisms were used and the same results were obtained. Therefore, below we will discuss only restricted DFT results. Furthermore, the B3LYP/6-311G(d) and B3LYP/6-311+G(d) approaches provide very close results, and therefore, below we will discuss only B3LYP/6-311+G(d) data, while we include the B3LYP/6-311G(d) results in Supporting Information (Table S4).

In the second part of the paper we further elaborate the role of electronic and steric effects of the substituent R of the pyridine rings in low-lying electronic states of the [(BPMEN)FeX$_2$]$^{2+}$ complex. For this purpose we performed B3LYP/LANL2DZ calculations of the geometry and energetics of complexes **3** (R = SiH$_3$), **4** (R = OH), **5** (R = F), **6** (R = CN), and **7** (R = *t*-Bu).

In the last, third, part of this paper we test the reliability of the above-presented density functional approximations. For this purpose we calculated the geometries and energy differences between close-lying electronic states of the model complex **8** at different levels of theory. Compound **8** was derived, for computational convenience, from complex **1**, by replacing (a) the ethylendiamine moiety by two ammonium molecules, (b) the acetonitrile ligands by the hydrogen cyanide molecules, and (c) the pyridine moieties by imines. Here we used hybrid B3LYP, nonhybrid BLYP, Hartree−Fock (HF), second-order frozen-core Møller−Plesset (MP2),[18] and coupled cluster method including single, double,[19] and perturbative triple excitations (CCSD(T)).[20] We also analyzed the basis set effects by performing B3LYP and MP2 calculations using the LANL2DZ, 6-311+G(d), and 6-311+G(3df,p) basis sets.

In all the calculations of the [(BPMEN)FeX$_2$]$^{2+}$ complex we used X = NCCH$_3$. All calculations were carried out with Gaussian 98[21] and Gaussian 03[22] program packages.

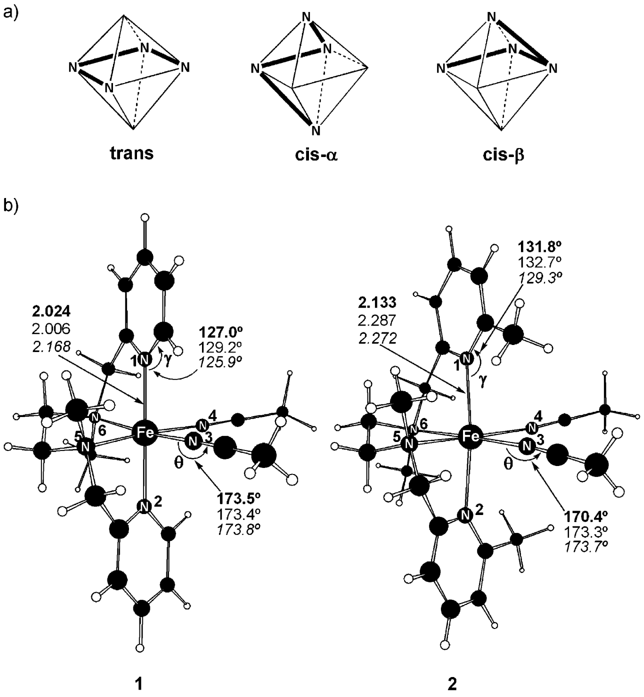

Figure 2. (a) Three possible different topologies of tetradentate N4 ligands in transition metal complexes and (b) fully optimized geometries (distances in angstroms and angles in degrees) for **1** and **2**. Numbers in bold, plain, and italic styles correspond to LS, IS, and HS values, respectively.

3. Results and Discussion

A. Geometries, Electronic Structure, and Energetics of Complexes 1 and 2. In general, low-lying electronic states of the [(BPMEN)FeX$_2$]$^{2+}$ complex may have singlet (low spin, LS), triplet (intermediate spin, IS), and quintet (high spin, HS) spin multiplicities. Below, we will study geometries and energetics of complexes **1** and **2** in all these spin states.

Let us start our discussions with the geometric structures of complexes **1** and **2**. In principle, a tetradentate ligand such as BPMEN in these complexes can adopt three different topologies, trans, cis-α, and cis-*β* (Figure 2a).[23] However, only the cis-α conformation was observed experimentally, where the tetradentate ligand adopts the position with the two pyridine rings coordinated to the transition metal center trans to each other. For example, the X-ray structure of **2** with two terminal triflate anions (X = $^-$OSO$_2$CF$_3$) contains the cis-α conformation of BPMEN. Therefore, in our studies we chose the cis-α conformation of BPMEN, and will not discuss other possible conformers.

Two important structural features that determine the properties of these Fe(II) complexes are the Fe−ligand distance and the distortion of the BPMEN polyhedron, which can be described by the angle N^i−Fe−N^j (β), where N^i and N^j stand for different nitrogen atoms of the ligands attached to the Fe center. The view of the fully optimized complexes **1** and **2** in Figure 2b shows that the cations [Fe(BPMEN)(CH$_3$CN)$_2$]$^{2+}$ and [Fe(6-Me$_2$-BPMEN)(CH$_3$CN)$_2$]$^{2+}$ have distorted octahedral geometries in all spin states. (Full

---

[18] Møller, C.; Plesset, M. S. *Phys. Rev.* **1934**, *46*, 618.

[19] Purvis, G. D.; Bartlett, R. J. *J. Chem. Phys.* **1982**, *76*, 1910.

[20] Raghavachari, K.; Trucks, G. W.; Pople, J. A.; Head-Gordon, M. *Chem. Phys. Lett.* **1989**, *157*, 479.

[21] Frisch, M. J.; Trucks, G. W.; Schlegel, H. B.; Scuseria, G. E.; Robb, M. A.; Cheeseman, J. R.; Zakrzewski, V. G.; Montgomery, J. A., Jr.; Stratmann, R. E.; Burant, J. C.; Dapprich, S.; Millam, J. M.; Daniels, A. D.; Kudin, K. N.; Strain, M. C.; Farkas, O.; Tomasi, J.; Barone, V.; Cossi, M.; Cammi, R.; Mennucci, B.; Pomelli, C.; Adamo, C.; Clifford, S.; Ochterski, J.; Petersson, G. A.; Ayala, P. Y.; Cui, Q.; Morokuma, K.; Malick, D. K.; Rabuck, A. D.; Raghavachari, K.; Foresman, J. B.; Cioslowski, J.; Ortiz, J. V.; Stefanov, B. B.; Liu, G.; Liashenko, A.; Piskorz, P.; Komaromi, I.; Gomperts, R.; Martin, R. L.; Fox, D. J.; Keith, T.; Al-Laham, M. A.; Peng, C. Y.; Nanayakkara, A.; Gonzalez, C.; Challacombe, M.; Gill, P. M. W.; Johnson, B. G.; Chen, W.; Wong, M. W.; Andres, J. L.; Head-Gordon, M.; Replogle, E. S.; Pople, J. A. *Gaussian 98*, revision A.11; Gaussian, Inc.: Pittsburgh, PA, 1998.

[22] Frisch, M. J.; Trucks, G. W.; Schlegel, H. B.; Scuseria, G. E.; Robb, M. A.; Cheeseman, J. R.; Montgomery, J. A., Jr.; Vreven, T.; Kudin, K. N.; Burant, J. C.; Millam, J. M.; Iyengar, S. S.; Tomasi, J.; Barone, V.; Mennucci, B.; Cossi, M.; Scalmani, G.; Rega, N.; Petersson, G. A.; Nakatsuji, H.; Hada, M.; Ehara, M.; Toyota, K.; Fukuda, R.; Hasegawa, J.; Ishida, M.; Nakajima, T.; Honda, Y.; Kitao, O.; Nakai, H.; Klene, M.; Li, X.; Knox, J. E.; Hratchian, H. P.; Cross, J. B.; Adamo, C.; Jaramillo, J.; Gomperts, R.; Stratmann, R. E.; Yazyev, O.; Austin, A. J.; Cammi, R.; Pomelli, C.; Ochterski, J. W.; Ayala, P. Y.; Morokuma, K.; Voth, G. A.; Salvador, P.; Dannenberg, J. J.; Zakrzewski, V. G.; Dapprich, S.; Daniels, A. D.; Strain, M. C.; Farkas, O.; Malick, D. K.; Rabuck, A. D.; Raghavachari, K.; Foresman, J. B.; Ortiz, J. V.; Cui, Q.; Baboul, A. G.; Clifford, S.; Cioslowski, J.; Stefanov, B. B.; Liu, G.; Liashenko, A.; Piskorz, P.; Komaromi, I.; Martin, R. L.; Fox, D. J.; Keith, T.; Al-Laham, M. A.; Peng, C. Y.; Nanayakkara, A.; Challacombe, M.; Gill, P. M. W.; Johnson, B.; Chen, W.; Wong, M. W.; Gonzalez, C.; Pople, J. A. *Gaussian 03*, Revision B.01; Gaussian, Inc.: Pittsburgh, PA, 2003.

[23] (a) Aldrich-Wright, J. R.; Vagg, R. S.; Williams, P. A. *Coord. Chem. Rev.* **1997**, *166*, 361. (b) Knof, U; Zelewsky, A. v. *Angew. Chem. Int. Ed.* **1999**, *38*, 302. (c) Ng, C.; Sabat, M.; Fraser, C. L. *Inorg. Chem.* **1999**, *38*, 5545.

Table 1. B3LYP/LANL2DZ Optimized and Experimental Iron−Ligand (Fe−N^{i})[a] Bond Lengths (in angstroms) for Various Spin States of Compounds **1**−**7**

compound		Fe−N^{1}	Fe−N^{2}	Fe−N^{3}	Fe−N^{4}	Fe−N^{5}	Fe−N^{6}
1	^{1}A	2.024	2.024	2.013	2.014	2.076	2.076
	^{3}A	2.006	2.006	2.250	2.251	2.203	2.203
	^{5}A	2.168	2.170	2.292	2.291	2.250	2.251
	X-ray	2.002(4)	2.015(4)	1.950(5)	1.942(5)	2.053(5)	2.055(5)
2	^{1}A	2.133	2.134	2.017	2.016	2.083	2.084
	^{3}A	2.287	2.374	1.989	2.210	2.168	2.055
	^{5}A	2.272	2.272	2.297	2.294	2.247	2.248
	X-ray[b]	2.2899(19)	2.2900(19)	2.1061(15)[c]	2.1062(15)[c]	2.2189(19)	2.2189(19)
3	^{1}A	2.140	2.138	2.013	2.016	2.076	2.077
	^{5}A	2.315	2.307	2.273	2.271	2.235	2.233
4	^{1}A	2.083	2.086	2.009	2.009	2.069	2.068
	^{5}A	2.228	2.230	2.266	2.266	2.241	2.243
5	^{1}A	2.006	2.067	2.011	2.010	2.071	2.071
	^{5}A	2.236	2.234	2.250	2.250	2.240	2.238
6	^{1}A	2.106	2.104	2.010	2.009	2.072	2.073
	^{5}A	2.294	2.295	2.228	2.228	2.232	2.231
7	^{1}A	2.409	2.401	2.012	2.011	2.079	2.080
	^{5}A	2.545	2.572	2.233	2.233	2.236	2.229

[a] For atomic labels, see Figure 2b. [b] Crystal structure corresponding to [(BPMEN)Fe(OTf)$_2$] with R = Me. [c] Bond distances between the Fe center and triflate oxygen atom.

Table 2. Relative Energy (Δ*E*), $\langle S^2 \rangle$ Expectation Value, and Mulliken Spin Density on Fe (spin$_{Fe}$) for Compounds **1** and **2** at B3LYP/LANL2DZ Optimized Geometries

		compound **1**			compound **2**		
method	state	Δ*E* (kcal/mol)	$\langle S^2 \rangle$	spin$_{Fe}$	Δ*E* (kcal/mol)	$\langle S^2 \rangle$	spin$_{Fe}$
B3LYP/LANL2DZ	^{1}A	2.1	0.00	0.00	9.5	0.00	0.00
	^{3}A	11.4	2.02	2.01	16.1	2.02	2.01
	^{5}A	0.0	6.01	3.79	0.0	6.01	3.81
B3LYP/6-311+G(d)	^{1}A	0.3	0.00	0.00	7.1	0.00	0.00
	^{3}A	17.7	2.02	1.97	12.7	2.02	1.76
	^{5}A	0.0	6.01	3.70	0.0	6.01	3.45
B3PW91/LANL2DZ	^{1}A	5.1	0.00	0.00	12.3	0.00	0.00
	^{3}A	13.2	2.03	2.04	17.3	2.02	2.04
	^{5}A	0.0	6.01	3.84	0.0	6.01	3.86
BPW91/LANL2DZ	^{1}A	0.0	0.00	0.00	0.0	0.00	0.00
	^{3}A	16.7	2.04	2.08	5.9	2.03	2.06
	^{5}A	15.7	6.01	3.76	6.9	6.01	3.79
BLYP/LANL2DZ	^{1}A	0.0	0.00	0.00	0.0	0.00	0.00
	^{3}A	22.9	2.07	2.03	3.3	2.03	2.01
	^{5}A	17.8	6.01	3.70	10.3	6.01	3.72
PW91PW91/LANL2DZ	^{1}A	0.0	0.00	0.00	0.0	0.00	0.00
	^{3}A	18.6	2.04	2.07	14.7	2.03	2.05
	^{5}A	19.0	6.01	3.75	10.2	6.01	3.78

geometric parameters of these complexes are given in Tables S1 and S2 of the Supporting Information.) These results show that the degree of distortion is largest in the quintet ^{5}A state.

As seen in Table 1, the Fe−N bond distances are found to be the largest in the HS ^{5}A state and the shortest in the ^{1}A state. The comparison of the calculated and experimentally reported values for the Fe−N bond distances shows that the experimental values are closer to the calculated values for the LS state of **1** and HS (or IS) state of **2**, respectively. Furthermore, the calculated and experimental values of the Fe−N bond distances are, in general, in good agreement, except for those for Fe−N^{3} and Fe−N.^{4} (The calculated Fe−N^{3} and Fe−N^{4} bond lengths of **2** cannot be compared with the experimental Fe−O bond distances.) Comparison of the geometries for **1** and **2** shows that the inclusion of methyl groups in the 6-position of the two pyridine rings mainly affects Fe−N^{1} and Fe−N^{2} bond lengths; these bond distances are significantly longer for **2** than for **1**. This effect can be attributed to the steric repulsion of the methyl groups from the acetonitrile moieties (X), which is also reflected by the increase of angle γ, Fe−N^{1}−C, by 4.8°−3.5° and the decrease of angle θ, Fe−N^{3}−C, by 0.1°−3.1° upon going from **1** to **2** (Figure 2b).

As seen in Table 2, where we present the calculated relative energies of low-lying electronic states of complexes **1** and **2**, the ground electronic state of **1** is the HS state ^{5}A. However, its low spin state ^{1}A lies only 2.1 and 0.3 kcal/mol higher in energy at the B3LYP/LANL2DZ and B3LYP/6-311+G(d) levels, respectively. Thus, these calculations clearly show that the LS, ^{1}A, and HS, ^{5}A, states of complex **1** are almost degenerate, which is consistent with the available experimental data. Complex **2** with the methyl substituents at the 6-position of the two pyridine rings clearly favors the HS, ^{5}A, state; the ^{5}A state is calculated to be 9.5 and 7.1 kcal/mol more favorable than the ^{1}A state at the B3LYP/LANL2DZ and B3LYP/6-311+G(d) levels, respectively. This finding is consistent with the experimental observations. Triplet states are located at much higher energy for both complexes, and we will not discuss them in detail. One finds that the smaller basis set B3LYP/LANL2DZ and the larger basis set B3LYP/6-311+G(d) give the same conclusion on the spin states for both **1** and **2**. Therefore, the LANL2DZ basis set will be used for the study of complexes **3**−**8** at the B3LYP level.

In the literature it is reported that the hybrid DFT approach overestimates the high spin states of the transition metal complexes.[12] Reiher and co-workers[24] attribute this failure to the fact that the HS state is systematically favored in the Hartree−Fock theory, which includes the Fermi correlation between the same spin states but not the Coulomb correlation.[12,25] To address this problem, we have studied complexes **1** and **2** with five different density functionals, B3LYP, BLYP, B3PW91, BPW91, and PW91PW91, with the same LANL2DZ basis set. The results of these calculations are shown in Table 2.

As can be derived from Table 2, both hybrid functionals, B3LYP and B3PW91, agree with each other on the ordering of the energy of spin states (^{5}A < ^{1}A < ^{3}A), predicting the quintet ground state for both **1** and **2**. The LS−HS energy splitting is a few kilocalories per mole larger at the B3PW91 level than at the B3LYP level. Meanwhile, all the nonhybrid density functionals used (BPW91, BLYP, and PW91PW91) favor the low spin state, ^{1}A, which lies significantly lower than the HS state (15−19 kcal/mol for **1** and 7−10 kcal/mol for **2**). This conclusion for **2** contradicts the available experimental data that indicate the high spin ground state for this complex. Furthermore, although the prediction of the low spin ground state for **1** is in agreement with the experiment performed below −40 °C, the calculated LS−HS splitting (15.7−19.0 kcal/mol) can be considered excessively large in view of the reported spin-crossover for **1** at the −40 to 30 °C temperature range. These results indicate an extreme underestimation of the stability of the high spin state at the nonhybrid density functional levels. Thus, comparison of the calculated hybrid and nonhybrid density functional results for complexes **1** and **2** with the experiment data favors the hybrid methods. Although the accuracy of hybrid DFT methods in describing relative energies of close-lying electronic states in general may still constitute a question, here we found that the B3LYP functional satisfactorily describes the low-lying states of the complexes **1** and **2**.

Table 2 also includes the calculated Mulliken spin densities on Fe atom and the expectation value of the total spin operator S^2. Usually the unrestricted Hartree−Fock wave function is no longer a true eigenfunction of the total spin operator because HS states mix into the LS state. Therefore, an inspection of the spin contamination is mandatory to determine the correctness of the calculations: if the expectation value of $\langle S^2 \rangle$ is much greater than 0.0 for singlet, 2.0 for triplet, and 6.0 for quintet, the results are questionable and should be used with caution. As seen in Table 2, for unrestricted singlet states the $\langle S^2 \rangle$ values are 0.00, converging to a restricted solution. It ranges within 2.02−2.03 and 6.01−6.02 for the triplet and quintet states, respectively. Spin density analysis show that almost all the spin remains on the iron center.

Table 3. B3LYP/LANL2DZ Relative Energy (ΔE), $\langle S^2 \rangle$ Expectation Value, and Mulliken Spin Density on Fe (spin$_{\text{Fe}}$) for Compounds **1**−**7** at the Respectively Optimized Geometries at the Same Level

compound	R	state	ΔE (kcal/mol)	$\langle S^2 \rangle$	spin$_{\text{Fe}}$
1	H	^{1}A	2.1	0.00	0.00
		^{5}A	0.0	6.01	3.79
2	CH$_3$	^{1}A	9.5	0.00	0.00
		^{5}A	0.0	6.01	3.81
3	SiH$_3$	^{1}A	8.5	0.00	0.00
		^{5}A	0.0	6.01	3.81
4	OH	^{1}A	5.3	0.00	0.00
		^{5}A	0.0	6.01	3.81
5	F	^{1}A	5.1	0.00	0.00
		^{5}A	0.0	6.01	3.80
6	CN	^{1}A	6.3	0.00	0.00
		^{5}A	0.0	6.01	3.80
7	*t*-Bu	^{1}A	17.9	0.00	0.00
		^{5}A	0.0	6.01	3.83

B. Substituent Effects on Geometries, Electronic Structure, and Energies of Complex 1. Discussion in the preceding section showed that LS and HS states of complex **1** (R = H) are almost energetically degenerate with a slight preference for the HS state. Substitution of H ligands at the 6-position of the two pyridine rings by methyl groups (i.e., upon going from complex **1** to complex **2**) stabilizes the HS state of the complex. To further investigate the effect of the substituent R on the electronic and geometric structures of the [(BPMEN)Fe(NCCH$_3$)$_2$]$^{2+}$ complex, we extend our studies to complexes **3**−**7** (see Figure 1), with the σ (R = SiH$_3$), **3**, and π (R = OH), **4**, electron donating, as well as the σ (R = F), **5**, and π (R = CN), **6**, electron withdrawing groups. We also studied complex **7**, with the bulky R = *t*-Bu group. To our knowledge, there are no experimental results for complexes **3**−**7**.

The LS and HS states of these complexes were investigated, and all of them were found to have distorted octahedral geometries similar to those in **1** and **2**. As shown in Table 1, the Fe−N bond distances are in general larger for the HS than for the LS state. The substituents at the 6-position of the two pyridine rings affect the Fe−N^1 and Fe−N^2 bond distances most significantly. Regardless of the nature of the substituents and the spin state of the complex, the Fe−N^1 and Fe−N^2 bonds are elongated upon substitution, except the LS state of **6**, where CN substituent shortens the Fe−N^1 bond by 0.02 Å. The Fe−N^1 and Fe−N^2 elongation is within the range of 0.05−0.15 Å for **2**−**5**, and has no clear correlation with the electronic nature of the substituents. The largest elongation of the Fe−N^1 and Fe−N^2 bonds, 0.38−0.40 Å, were obtained for **7** with the bulkiest *t*-Bu substituent. The latter effect clearly can be attributed to the steric repulsion between the *tert*-butyl groups and the acetonitrile ligands. Indeed, the characteristic γ angle, defined in Figure 2b, in **7** (138° and 139° for HS and LS, respectively) is significantly, 12°, larger than the corresponding one for **1**.

As seen in Table 3, any R substitution in the 6-position favors the HS state. The LS−HS energy splitting is 9.5, 8.5, 5.3, 5.1, 6.3, and 17.9 kcal/mol for the complexes **2** (R = CH$_3$), **3** (R = SiH$_3$), **4** (R = OH), **5** (R = F), **6** (R = CN),

---

(24) (a) Salomon, O.; Reiher, M.; Hess, B. A. *J. Chem. Phys.* **2002**, *117*, 4729-4737. (b) Reiher, M. *Inorg. Chem.* **2002**, *41*, 6928−6935.

(25) Harris, D.; Loew, G. H.; Komornicki, A. *J. Phys. Chem. A* **1997**, *101*, 3959−3965.

Table 4. Optimized Iron−Ligand Bond Lengths (in angstroms) for Model Compound **8**, Using LANL2DZ Basis Set

method	state	Fe−N^1	Fe−N^2	Fe−N^3	Fe−N^4	Fe−N^5	Fe−N^6
B3LYP	^{1}A	2.006	2.006	1.980	1.980	2.061	2.061
	^{5}A	2.200	2.200	2.348	2.348	2.212	2.212
MP2	^{1}A	2.040	2.040	2.025	2.025	2.088	2.088
	^{5}A	2.234	2.235	2.338	2.332	2.252	2.253

Table 5. Relative Energy (Δ*E*), $\langle S^2\rangle$ Expectation Value, and Mulliken Spin Density on Fe (spin$_{Fe}$) for Model Compound **8**, at B3LYP/LANL2DZ Optimized Geometries

		LANL2DZ^a			6-311+G(d)^a			6-311+G(3df,p)^a		
method	state	Δ*E* (kcal/mol)	$\langle S^2\rangle$	spin$_{Fe}$	Δ*E* (kcal/mol)	$\langle S^2\rangle$	spin$_{Fe}$	Δ*E* (kcal/mol)	$\langle S^2\rangle$	spin$_{Fe}$
B3LYP	^{1}A	1.6	0.00	0.00	1.0	0.00	0.00	1.3	0.00	0.00
	^{5}A	0.0	6.01	3.79	0.0	6.01	3.71	0.0	6.01	3.69
BLYP	^{1}A	−19.0	0.00	0.00						
	^{5}A	0.0	6.01	3.71						
HF	^{1}A	81.5	0.00	0.00						
	^{5}A	0.0	6.04	3.95						
MP2	^{1}A	39.7	0.00	0.00	27.6	0.00	0.00	21.2	0.00	0.00
	^{5}A	0.0	6.04	3.95	0.0	6.01	3.87	0.0	6.01	3.87
CCSD	^{1}A	31.9	0.00	0.00						
	^{5}A	0.0	6.03	3.95						
CCSD(T)	^{1}A	24.9	0.00	0.00						
	^{5}A	0.0	6.03	3.95						

^{a} Basis set.

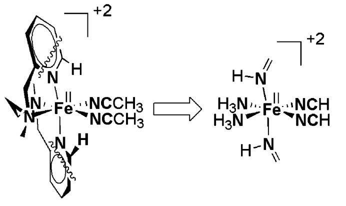

Compound **1**   Model compound **8**

Figure 3. Representation of simplifications done to compound **1** leading to model compound **8**.

and **7** (R = *t*-Bu), respectively. For all these complexes the ground state is the HS state. These results indicate that any R substituent (regardless of σ- or π-electron withdrawing or donating) larger than H stabilizes the HS state of (BPMEN)-FeX$_2$ complexes. Moreover, the prediction for compound **7**, 17.9 kcal/mol, confirms that steric effects have an important contribution to the LS−HS splitting energy.

C. Reliability of the Theoretical Approximations and the Models. As demonstrated above, hybrid density functional methods (such as B3LYP) provide a better description of the relative energies of low-lying electronic states of $[(BPMEN)Fe(NCCH_3)_2]^{2+}$ systems than their nonhybrid analogues. Here we further elaborate the accuracy of the B3LYP method in describing relative energies of the low-lying electronic states of $[(BPMEN)Fe(NCCH_3)_2]^{2+}$ systems by performing calculations with high level ab initio methods: the second-order Møller−Plesset, MP2, and the single and double coupled cluster without and with perturbative inclusion of the triple excitations, CCSD and CCSD(T), for the model complex **8**, derived from complex **1**, as explained under Computational Methods and shown in Figure 3. The geometry of this complex was optimized at the B3LYP/LANL2DZ and MP2/LANL2DZ levels.

As seen in Table 4, B3LYP/LANL2DZ optimized geometries of complex **8** are very close to those of real complex **1**, indicating that **8** is a good model of complex **1**. Furthermore, B3LYP/LANL2DZ and MP2/LANL2DZ methods provide similar results. Therefore, we used the B3LYP/LANL2DZ optimized geometries for high level single point calculation.

In Table 5 we present results of single point calculations at B3LYP, BLYP, HF, MP2, CCSD, and CCSD(T) at B3LYP/LANL2DZ optimized geometries for model complex **8**. The B3LYP calculated splitting between the low-lying states of complex **8** are in good agreement with those computed for the real system **1**; the energy splitting, 1.6 kcal/mol, between LS and HS for model system **8** are very close to that, 2.1 kcal/mol, for real system **1**. This comparison once again demonstrates that complex **8** is good model of **1**.

As seen in Table 5, the nonhybrid BLYP method alters HS and LS states in the energy scale and makes LS lower by 19.0 kcal/mol compared to hybrid B3LYP method. As stated before, this is due to the overestimation of the stability of the higher spin states by the Hartree−Fock (HF) method in hybrid DFT approaches. Indeed, as seen in Table 5 the HF method dramatically, by 81 kcal/mol, stabilizes the ^{5}A state with respect to the ^{1}A state. Therefore, it is expected that any method based on HF wave function will favor the high spin state.

Indeed, the MP2 and CC methods, like hybrid density functional B3LYP, predict the high spin ground state for complex **8**. However, in contrast to the B3LYP method, these post-HF methods predict a very large energy difference between the LS and HS states. At the MP2 level the LS−HS splitting is about 40 kcal/mol, while it is 31.9 kcal/mol at the CCSD level. In other words, CCSD method reduces the LS−HS energy splitting by 8 kcal/mol. The inclusion of the triplet excitations into the calculations additionally reduces it by 7 kcal/mol: from 31.9 kcal/mol at the CCSD level to 24.9 kcal/mol at the CCSD(T) level. At the end, CCSD(T) calculated LS−HS splitting for complex **8** is 15 kcal/mol smaller than that obtained at the MP2 level.

In the literature[26] it is well accepted that the CCSD(T) method provides results that are close to the experiment. However, the basis set LANL2DZ used in our CCSD(T) calculations is expected to be not large enough to fully account for electronic correlation effects. Therefore, we studied the basis set effects by performing B3LYP and MP2 calculations using much larger basis sets 6-311+G(d) and 6-311+G(3df,p) (which includes the 3df polarization functions on Fe atom, d polarization functions on N and C atoms, and p polarization functions on H). The results are summarized in Table 5. As seen from this table, the B3LYP results are not basis set sensitive. However, a substantial relative energy drop is observed at the MP2 level upon going from LANL2DZ to the larger basis sets 6-311+G(d) and 6-311+G(3df,p): from 39.7 kcal/mol to 27.6 and 21.1 kcal/mol, respectively. Thus, improving the basis set from LANL2DZ to 6-311+G(3df,p) reduces the MP2 calculated LS−HS splitting by almost 18.6 kcal/mol! Since we were not able to calculate LS−HS splitting at the CCSD(T) level with the large 6-311+G(3df,p) basis set, we assumed the same basis set effect dependence for CCSD(T) as for MP2, in the same spirit as in G2 and G2M procedures.[27] Using this assumption, we roughly estimated the CCSD(T)/6-311+G(3df,p) LS−HS energy splitting to be about 5−6 kcal/mol, which is close to the B3LYP/LANL2DZ calculated data. Therefore, for lack of CCSD(T) results with larger basis sets, we expect that the B3LYP/LANL2DZ method used in this paper provides a reasonable qualitative description of the low-lying electronic states of the $(BPMEN)FeX_2$ complexes.

3. Conclusions

From the above-presented discussions we can draw the following conclusions:

1. The hybrid B3LYP method provides a qualitatively accurate description of the low-lying electronic states of $[(BPMEN)Fe(NCCH_3)_2]^{2+}$ complexes. In contrast, the nonhybrid DFT methods (such as BLYP, BPW91, and PW91PW91) incorrectly describe the low-lying states of these complexes.

2. The low-lying high spin and low spin states of complex **1**, with the H ligands in the 6-position of two pyridine rings of BPMEN, are almost degenerate with a slight preference for the high spin state. The substitution of the H ligands in the 6-position with other R groups favors the HS states: the calculated LS−HS energy splitting is 9.5, 5.3, 8.5, 6.3, and 5.1 kcal/mol for complexes **2** ($R = CH_3$), **3** ($R = SiH_3$), **4** ($R = OH$), **5** ($R = F$), and **6** ($R = CN$), respectively. For all these complexes the ground state is the HS state. Any R substituent (regardless of σ- or π-electron withdrawing or donating) larger than H stabilizes the HS state of $(BPMEN)FeX_2$ complexes. Our findings for complexes **1** and **2** are in good agreement with the experimental observations.

3. Meanwhile, the calculated LS−HS splitting, 17.9 kcal/mol, for complex **7** with R = *t*-Bu clearly demonstrates the importance of the steric effects in these complexes, which favors the high spin state.

Acknowledgment. D.Q. thanks the Ministerio de Educación, Cultura y Deporte for a postdoctoral grant. The present research is in part supported by a grant (CHE-0209660) from the National Science Foundation. Acknowledgment is made to the Cherry L. Emerson Center of Emory University for the use of its resources, which is in part supported by a National Science Foundation grant (CHE-0079627) and an IBM Shared University Research Award.

Supporting Information Available: Tables S1 and S2 show calculated angles β, the angle $N^i{-}Fe{-}N^j$ where N^i and N^j stand for different nitrogen atoms of the ligands attached to the Fe center, for **1** and **2**, respectively. Table S3 shows the absolute energy values for **1** and **2**, and Table S4 gives single point B3LYP/6-311G(d)//B3LYP/LANL2DZ absolute and relative energy values, $\langle S^2 \rangle$, and spin densities on Fe ($spin_{Fe}$) for **1** and **2**. Absolute energy values for **3**−**7** are presented in Table S5. Table S6 shows absolute energy values for our model compound **8**, and Table S7 consists of absolute and relative energy values, $\langle S^2 \rangle$, and spin densities on Fe ($spin_{Fe}$) for CCSD(T) calculations with the frozen core for model compound **8**. Table S8 includes the absolute energy values for the model compound **8** using different basis sets. Coordinates, in *xyz* format, of all compounds also have been included. This material is available free of charge via the Internet at http://pubs.acs.org.

IC0348392

---

(26) Ghosh, A; Taylor, P. R. *Curr. Opin. Chem. Biol.* **2003**, *7*, 113.

(27) Curtiss, L. A.; Raghavachari, K.; Trucks, G. W.; Pople, J. A. *J. Chem. Phys.* **1991**, *84*, 7221. (b) Froese, R. D. J.; Humbel, S.; Svensson, M.; Morokuma, K. *J. Phys. Chem. A* **1997**, *101*, 227.